

Novel Ti/Zr Based Non-Chromium Chemical Conversion Coating for the Corrosion Protection of Electrogalvanized Steel

Yong Guan, Jian-guo Liu, Chuan-wei Yan*

State Key Laboratory for Corrosion and Protection, Institute of Metal Research, Chinese Academy of Sciences, 62 Wencui Road, Shenyang 110016, China

*E-mail: cwyang@imr.ac.cn

Received: 7 August 2011 / Accepted: 29 August September 2011 / Published: 1 October 2011

A novel Ti/Zr based chemical conversion coating was developed for improving the corrosion resistance of electrogalvanized steel using fluotitanate acid, fluozirconate acid and hydrofluoric acid, etc. The surface morphology was investigated by SEM. Coating composition was analyzed using XPS and FTIR. EIS and potentiodynamic polarization curves were used to evaluate the corrosion behavior. The results showed that the conversion coating was compact with the thickness of about 500 nm, and had a uniform amorphous composition that consisted of nanoscale complicated oxides or hydroxides and zinc fluorides. The Ti/Zr based conversion coating exhibited a relatively better protection for the electrogalvanized steel because the corrosion current (I_{corr}) was about two orders of magnitude lower than the zinc coating substrate. EIS results indicated that the corrosion reaction of the prepared conversion coating was mixed-controlled by charge transition and diffusion charge during its three corrosion stages.

Keywords: Non-chromium, Ti/Zr based conversion coating, nanoscale, Corrosion resistance, Electrogalvanized steel

1. INTRODUCTION

Electrogalvanized steel has found widespread use in many applications [1]. The zinc coating protects steel matrix by providing a barrier to corrosive media and sacrificing nature of the coating. However, zinc itself undergoes corrosion leading to the formation of “white rust” on its surface that can be significantly affect the appearance as well as the organic coating adhesion.

Considering this, the corrosion resistance performance of zinc coating is usually improved by means of chemical conversion treatments. The traditional methods including chromate passivation and phosphating processes, unfortunately, have serious disadvantages on environmental contamination and

human health [2, 3], because the waste water and sludge contain not only heavy metals but also phosphorus that could cause water eutrophication. To cope with this problem, great efforts have therefore been made to alternative eco-friendly conversion coatings that using trivalent chromium [4], molybdate [5], rare earth [6, 7], silicate or silane [8-11].

In the last few years, a new generation of environment-friendly conversion coating that mainly based on titanium or zirconium oxides has attracted extensive attention owing to its good corrosion and wear resistance [12-14]. Moreover, the new conversion coatings can operate at lower temperature and generate significantly less sludge than phosphate processes. These Ti/Zr based conversion coatings have been mostly used for the aluminum and magnesium alloys surface treatment [15-18], however, the reports applying to the zinc are scarce up to now.

In the present paper, a novel Ti/Zr based non-chromium chemical conversion coating was developed for protecting the electrogalvanized steel. After the primary structure characterization of the conversion coating, the anticorrosion performance and the corrosion behavior were studied by electrochemical methods.

2. EXPERIMENTAL

2.1. Materials

The test panels were cold rolled low-carbon steel ($50 \times 50 \times 1$ mm). Firstly, these panels were alkaline degreased and rinsed thoroughly by deionized water. Then the steel sheets were electroplated by using alkaline non-cyanide zinc plating process to produce a bright zinc coating of which the thickness was about 10 μm .

2.2. Chemical Conversion Coating Preparation

The Ti/Zr based chemical conversion solution was prepared using fluotitanate acid (60 wt%, 5 g/L), fluozirconate acid (45 wt%, 7.5 g/L) and hydrofluoric acid (40 wt%, 0.2 g/L). Also, the solution is comprised of film-forming accelerators and pH stabilizers. The chemical conversion coating preparation steps were as follows:

(1) The pH value of the chemical conversion solution was adjusted to 3.0 ± 0.2 using KOH or $\text{NH}_3 \cdot \text{H}_2\text{O}$, and then the solution was heated to 45 ± 5 °C.

(2) The freshly prepared electrogalvanized steel panels were dipped into the chemical conversion solution for 90 s. After remaining in the air for 30 s, the panels were firstly rinsed thoroughly with running tap water and then deionized water.

(3) The converted panels were then dried with hot-air and taken to the oven with temperature of 50-60 °C for 30 minutes in order to age the conversion coatings.

2.3. Performance Tests

2.3.1. Morphological Analysis

The surface morphology of the conversion coating was carried out by FEI Inspect F (25 kV) Field Emission Gun Scanning Electron Microscope (FEG-SEM) equipped with Oxford INCA X-MAX 20 Energy Dispersive X-ray Spectroscopy (EDS) system.

2.3.2. Component Analysis

The chemical composition of the conversion coating was analyzed by X-ray Photoelectron Spectroscopy (XPS) with a Thermo VG Scientific ESCALAB 250 spectrometer. The spectra were collected with a monochromatic Al K α X-ray source (1486.6 eV). The depth profile analysis of the coating was conducted by argon ion sputtering with an ion gun voltage of 2 kV and current of 2 μ A for 10 min. Scanning steps of 1 and 0.2 eV \cdot step $^{-1}$ with an interval of 50 ms were utilized for survey and high-resolution modes.

The surface of the conversion coating was also investigated by a Nicolet Magna IR-560 Fourier Transform Infrared (FTIR) Spectrometer in the wavenumber range from 400 to 4000 cm^{-1} .

2.3.3. Electrochemical Characterization

The tested samples were evaluated by potentiodynamic polarization curves and Electrochemical Impedance Spectroscopy (EIS) using EG&G M273 Potentiostat combined with an M5210 Lock-in Amplifier. A three-electrode system was employed in the tests, which was assembled with test specimen as a working electrode, large area platinum sheet was used as an auxiliary electrode and saturated calomel electrode (SCE) as a reference electrode. The area of the working electrode exposed to the corrosive media was 0.531 cm^2 . All measurements were carried out in neutral 5 w/v% NaCl solution at ambient temperature, and potentials mentioned in this paper were all relative to the SCE. The bare electrogalvanized steel panels were tested instantly after exposure to the electrolyte, and the samples with conversion coating were pre-immersed in the electrolyte for 10 minutes to achieve the constant open circuit potential (OCP) before measurement. The potentiodynamic polarization curves were acquired by M352 software from -250 to +500 mV (Vs. OCP) with a scan rate of 0.5 $\text{mV}\cdot\text{s}^{-1}$. The EIS spectra were recorded with M398 software over a frequency range from 10^{-2} to 10^5 Hz with an AC amplitude of 5 mV at OCP. The corrosion resistance tests data were analyzed using CorrView and ZView softwares, respectively.

3. RESULTS AND DISCUSSION

3.1. Coating morphology analysis

It can be seen from Figure 1(a) that the substrate is coated with a uniform and compact conversion coating in which the particles are evenly dispersed, and the particle size is below 80 nm.

According to the results from cross section showed in Figure 1(b), the conversion coating has a good combination with the zinc coating substrate. The coating thickness is about 500 nm.

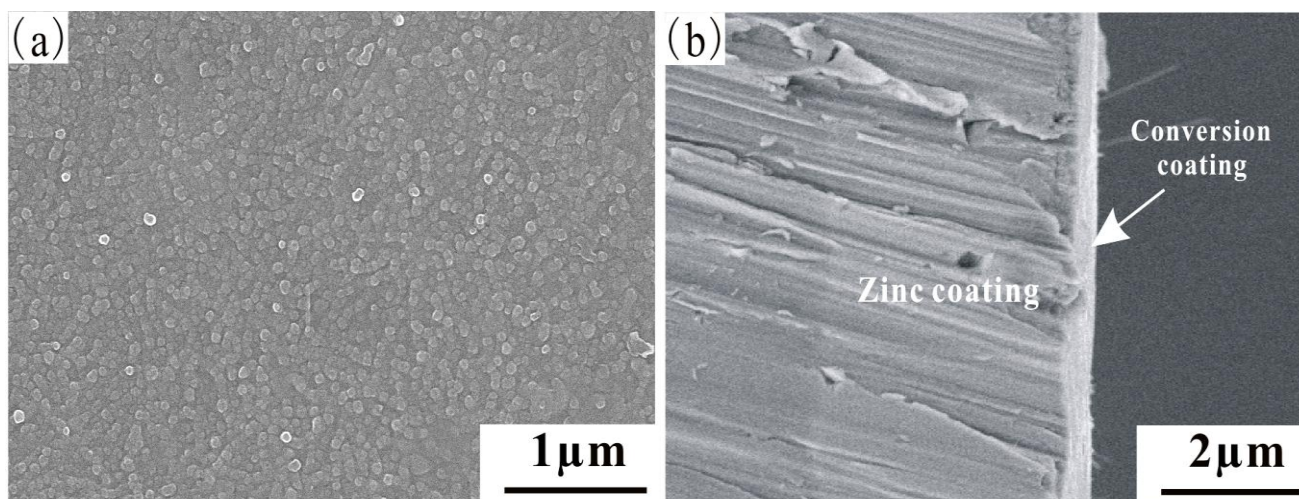


Figure 1. SEM micrographs of the surface of the Ti/Zr based conversion coating, (a) plan view, and (b) cross section.

3.2. Coating component analysis

Figure 2. displays the XPS survey and high-resolution spectra of the conversion coating after sputtered for 10 min by argon ion. The survey spectrum (Figure 2(a)) indicates that the presence of peaks related to Zn, Ti, Zr, O and F species. The F 1s peak (Figure 2(b)) at 685.2 eV is very close to F-Zn bonding (685.1 eV) in ZnF_2 [19]. The Zn 2p peaks (Figure 2(c)) consist of 2p_{3/2} and 2p_{1/2} spin-orbit components at 1022.2 and 1045.2 eV, which correspond to Zn-O bonding in ZnO [20, 21]. The Ti 2p (Figure 2(d)) spectrum was split into two main peaks due to the spin-orbital coupling of the 2p orbital, and each one can be fitted by two subprime peaks with different chemical shifts, 463.0 and 464.7 eV attributes to Ti 2p 1/2, 457.3 and 459.1 eV ascribe to Ti 2p 3/2. Moreover, 459.1 and 464.7 eV correspond to Ti^{4+} in TiO_2 , 457.3 and 463.0 eV may be correspond to Ti^{3+} in Ti_2O_3 [22,23].

The Zr 3d spectrum (Figure 2(e)) is comprised of three couples of peaks, the first peaks at the high binding energy can attribute to Zr 3d 3/2, and the other two couples at the low binding energy can attribute to Zr 3d 5/2. The peaks at 185.3, 184.8 and 183.3 eV correspond to Zr^{4+} in ZrO_2 [24], and the peaks at 182.8, 182.4 and 180.4 eV may be attributed to ZrO [25, 26]. The O 1s spectrum (Figure 2(f)) can be fitted by four peaks, the peaks at 530.0 and 530.6 eV respectively correspond to O-Zr bonding [27] and O-Zn bonding [28], the peak at 531.0 and 532.2 eV are related to O-Ti [29] and O-H bonding from absorbed water [30], respectively.

Figure 3 indicates that oxygen content is the highest in the overall five elements, which suggests that the conversion coating is mainly comprised of metal oxides or hydroxides. Comparing with other metal elements, the zinc content is much higher and increases remarkably, which indicates that zinc oxide or zinc hydroxide ought to be firstly generated, and then the zinc fluoride, titanium and

zirconium oxides or hydroxides are generated. With time prolonging, titanium and zirconium oxides or hydroxides dominate in the coating rather than zinc oxide or fluoride.

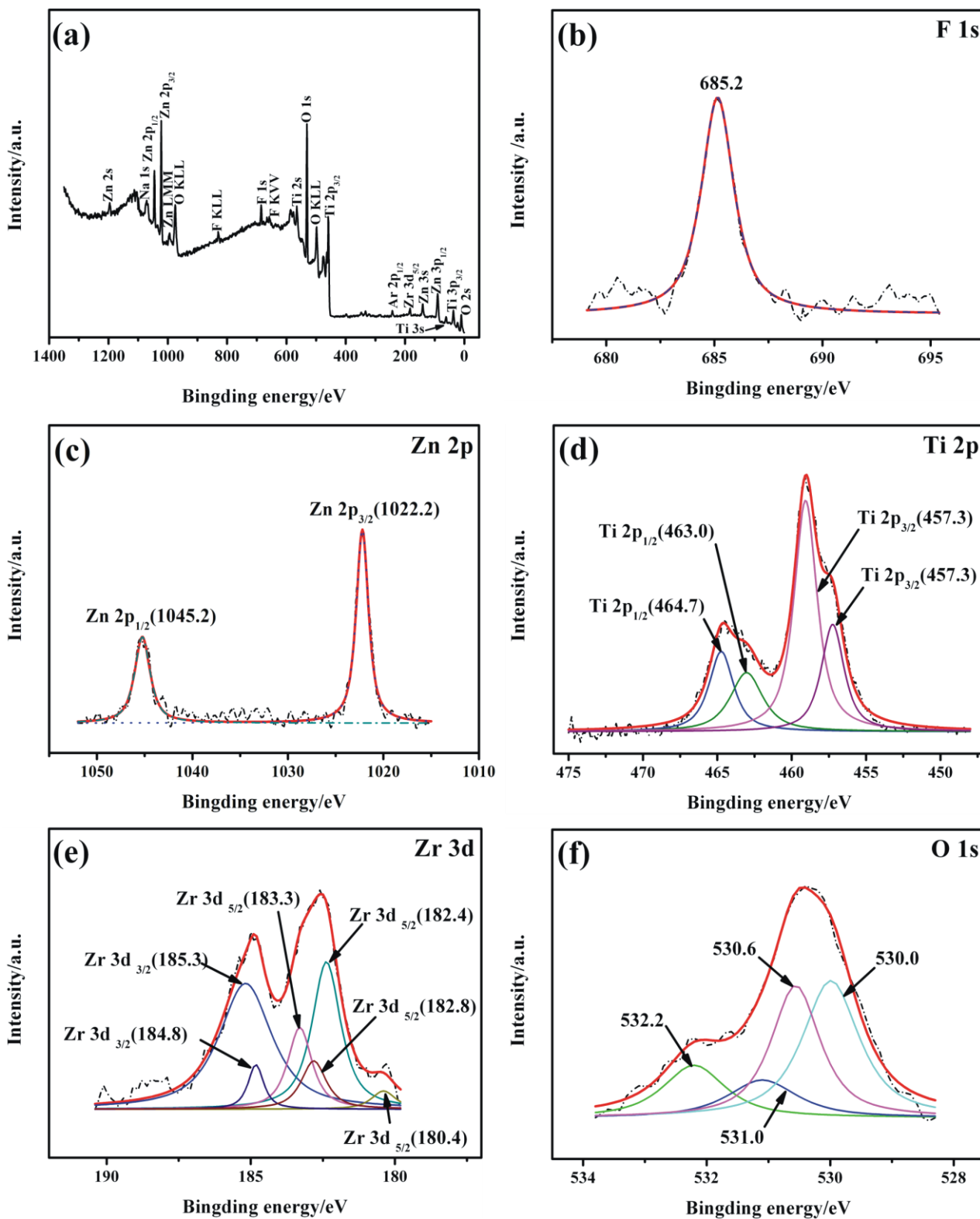


Figure 2. XPS spectra of the Ti/Zr based conversion coating after argon sputtering for 10 min, (a) survey spectrum, and (b-f) high-resolution spectra.

And comparing with the titanium, zirconium compounds grow faster and ultimately become the chief parts of the conversion coating. In the meantime, titanium content gradually drops off and is virtually the same as the zinc at last.

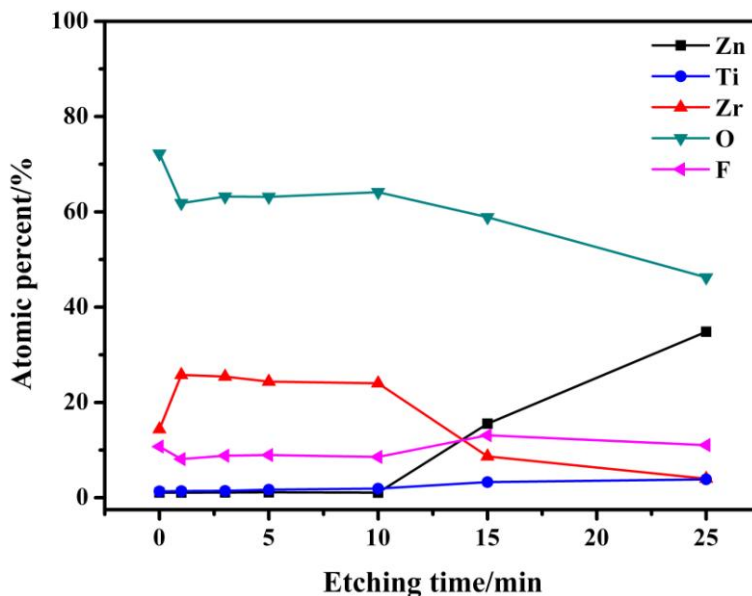


Figure 3. XPS depth profiling of the Ti/Zr based conversion coating.

According to the FTIR spectrum of the conversion coating showed in Figure 4, the peak near 671 cm^{-1} may be assigned to $-\text{OH}-\text{F}$ deformation vibration [31], and 938 cm^{-1} assigned to the bending vibration of $\text{O}-\text{Ti}-\text{O}$ [32].

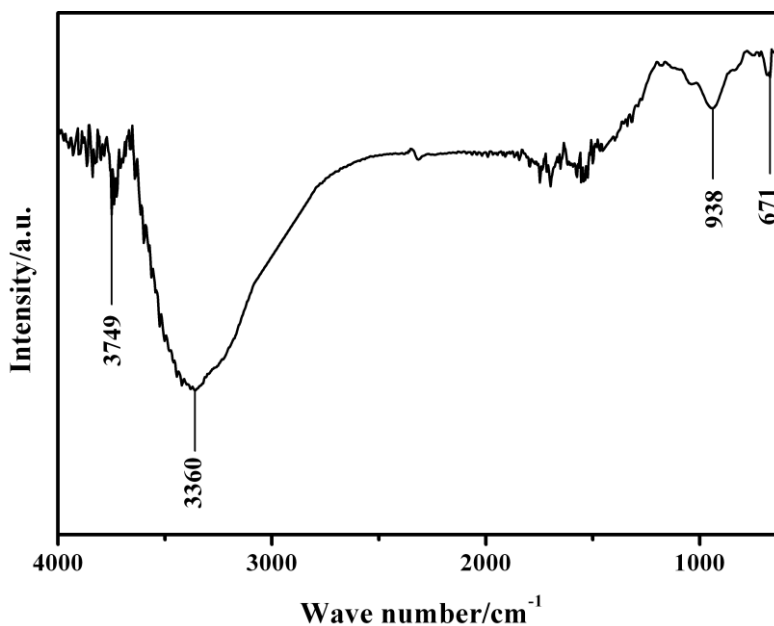


Figure 4. FTIR spectrum of the Ti/Zr based conversion coating.

The small peaks around 1500-1750 cm^{-1} can be assigned to frequencies of H-O-H bending vibrations [33], and the broad band centers at 3360 cm^{-1} corresponds to the stretching vibration of –OH, which suggests the crystal water existed in the conversion coating. The peak at 3750 cm^{-1} is due to the absorption of free hydroxyl on the surface of the conversion coating [34].

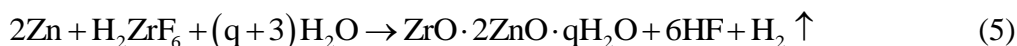
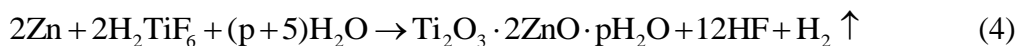
3.3. Coating forming mechanism

According to the results of the XPS and FTIR analysis, it can be deduced that the Ti/Zr based chemical conversion coating is consisted of zinc fluoride and zinc, titanium, zirconium oxides with crystal water. And the formation of the conversion coating can be made up of processes as follows:

(1) The first step is that zinc coating surface dissolves in the acidic conversion solution and forms zinc hydrated oxide, by which the hydrogen evolution and local pH value rising is accompanied.

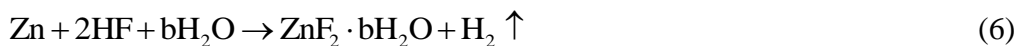


(2) Secondly, zinc reacts with fluotitanate and fluozirconate acids under the action of accelerants, and the hydrated titanium, zirconium oxides in different valence states and zinc oxide are generated, with which the hydrogen evolution is companied.



Among these compounds, the hydrates of ZnO, TiO_2 and ZrO_2 are the main phases, and the low valent hydrates of Ti_2O_3 , and ZrO could be the secondary phases.

(3) As the reacting time passed, the free hydrofluoric acid resulting from the last process becomes enriched in the conversion solution. Then the zinc coating may be reacted with the free hydrofluoric acid and generates hydrated zinc fluoride. At the same time, the zinc oxide included in the conversion coating could also be dissolved by the free hydrofluoric acid.



At the beginning stage of the coating formation, zinc oxide and zinc fluoride are the main compositions, and then the titanium or zirconium oxides become the dominating phases, especially the

zirconium oxides. Consequently, the substrate dissolution can be reduced enormously and the rapidly generated titanium or zirconium oxides can promote the compactness of conversion coating. Thus, the conversion coating could afford enough anticorrosion performance to the zinc coating substrate.

3.4. Electrochemical Characterization

Comparing with the zinc coating potentiodynamic polarization curve described in Figure 5, both the anodic and cathodic branches of the conversion coating show higher shift towards the low current density area. However, the anodic branch of the zinc coating presents a stronger active dissolution tendency, whereas the conversion coating exhibits a charge transition and diffusion mixed-controlled tendency to a certain degree. And meanwhile, the cathodic branch of the zinc coating shows a more obvious diffusion controlled tendency contrasted to the conversion coating, which indicates that the Ti/Zr based conversion coating is more inclined to inhibit the anodic corrosion [35]. It can be seen from Table 1 that the corrosion current (I_{corr}) of the conversion coating is about two orders of magnitude lower than the zinc coating, which reveals that the compact conversion coating has greatly reduced the corrosion rate of the zinc coating .

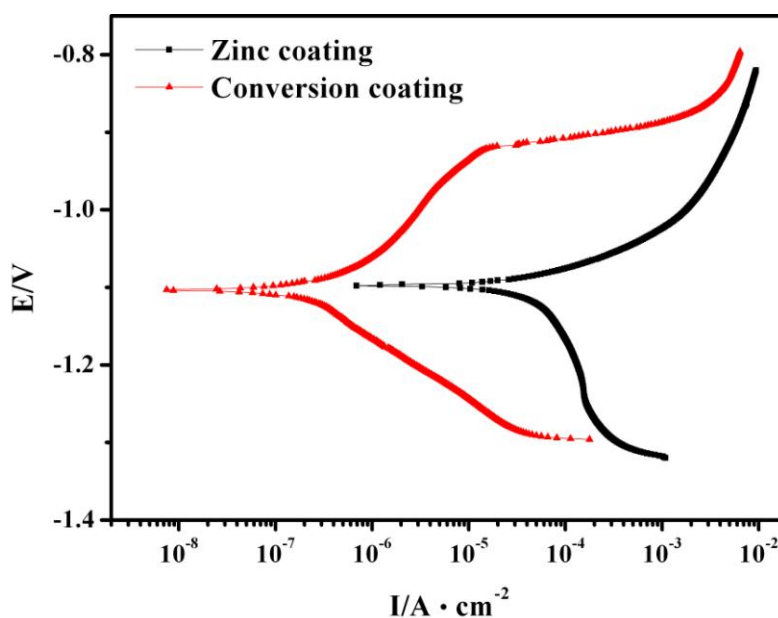


Figure 5. Potentiodynamic polarization curves of untreated and treated zinc coatings.

Table 1. Fitting results of potentiodynamic polarization curves in Figure 5.

	$I_{corr}/A \cdot cm^{-2}$	E_{corr}/V	$R_p/\Omega \cdot cm^2$	b_a/mV	b_c/mV
zinc coating	8.2146E-5	-1.0997	317.57	87.93	1030.2
conversion coating	4.7804 E-7	-1.1043	54570	121.87	116.69

The EIS plots of the untreated and treated zinc coatings for different immersion time are showed in Figure 6. The zinc coating has been corroded after immersed for 10 hours as the inductive reactance can be seen at the low frequency region (Figure 6(a)), which indicates the corrosion of the zinc coating substrate [36], and $|Z|$ has been decreased by about one order of magnitude.

Figure 6(b) to (d) show the EIS plots of the Ti/Zr based conversion coating at different immersion stages.

3.4.1. Initial stage

It can be seen that each Nyquist plot of Figure 6(b) is composed of one semicircle at the high frequency region and a straight line at an angle of about 45° in the low frequency region, which represent the capacitive arc and Warburg impedance, respectively. It is revealed that the corrosion reaction of conversion coating at the initial immersion stage is mixed-controlled by charge transition and diffusion. This result is in agreement with that obtained using potentiodynamic polarization curve as described above. With the immersion time extending, the radius of the capacitive arc at high frequency decreases. Furthermore, the $|Z|$ value also decreases by about one order of magnitude, with the phase angle decreasing and shifting toward higher frequency. It is indicated that the corrosion media continues to permeate through the conversion coating. The equivalent circuit of the initial immersion stage is inserted in the figure, and the fitting results are illustrated in Table 2. R_s is the solution resistance between the working electrode and reference electrode. The constant phase element (CPE) is used to replace the coating capacitance because of inhomogeneities presenting at microscale among the phases of the coating. R_c is the coating resistance. W_o represents the finite length Warburg diffusion impedance with an open circuit terminus, which usually means the barrier to the transport of ions into the coating due to good compactness of the coating [36]. The fitting results show the decrease of coating resistance and increase of coating capacitance, which indicates that the blocking performance of the conversion coating has been steadily dwindling. The decline of the anticorrosion performance is due to local microcracks formed on the conversion coating surface as showed in Figure 7(b).

3.4.2. Middle stage

The EIS plots of the conversion coating during the middle stage are showed in Figure 6(c). The Nyquist plots are also have capacitance arcs in the high frequency region and diffusion tails in the low frequency region. However, each of the capacitance arcs has been depressed seriously comparing with the first stage that is due to microscopic surface roughness or porousness of the coating, just as presented by Rammelt and Reinhard et.al. [37]. The Bode diagrams don't show obvious decline of the $|Z|$ value and phase angle at the medial immersion stage. The EIS data at this stage are analyzed using the equivalent circuit as shown in the inserted figure, and the fitting results are shown in Table 3. According to the suggestions proposed by Conde and Damborenea et.al. [38], the depressed capacitive arc in the high frequency region is composed of two capacitive loops. One of which in the higher

frequency region represents the capacitive arc of conversion coating, and the other is corresponding to the double layer. CPE_{dl} refers to the double layer capacitance, R_{ct} represents charge transfer resistance, and W_s is the finite length Warburg diffusion impedance with a short circuit terminus [36]. Comparing with the initial stage, the microcracks have propagated throughout the coating surface at the end of the middle stage (Figure 7(c)).

3.4.3. Final stage

Figure 6(d) describes the EIS plots of the conversion coating at the final immersion stage. The Nyquist plots in the high frequency region evolve into three loops gradually with the immersion time extending, corresponding to the Bode diagrams in the right figure reveal three time constants. The loop at the lowest frequency region corresponds to the corrosion products formed in the micropores or microcracks of the conversion coating. It is indicated that the conversion coating has been penetrated by the corrosive media and corrosion reacts on the zinc coating substrate. And the Warburg diffusion at the low frequency region may be due to the blocking function of corrosion products. The equivalent circuit is showed in the inserted figure and fitting results are in Table 4. For the reason of corrosion products generation, $|Z|$ value of the 18 day is a little higher than the 15 day. After immersing for 18 days, the protective action of the conversion coating has lost and corrosion products formed through the conversion coating cracks as shown in Figure 7(d) and (e).

The EIS data of the conversion coating illustrates that corrosion reaction of the whole immersion processing is mixed-controlled by charge transition and diffusion, which is in agreement with the potentiodynamic polarization curve analysis. During the immersion stages, as a result of the corrosive media, local microcracks firstly forms on the Ti/Zr based conversion coating, and then the corrosive media permeates through the microcracks and leads to the completely cracking. Finally, the anticorrosion performance of the conversion coating is completely damaged on account of the exposure of the zinc coating substrate.

Table 2. EIS fitting results of the conversion coating at the initial immersion stage.

	0d	1d	3d
$R_s(\Omega \cdot \text{cm}^2)$	23.99	22.62	20.12
$CPE_c-T(\Omega^{-1} \cdot \text{cm}^{-2} \cdot \text{s}^{-n})$	1.5429E-5	2.0823E-5	4.4901E-5
CPE_c-P	0.83345	0.77013	0.64502
$R_c(\Omega \cdot \text{cm}^2)$	14778	7402	2849
$W_o-R(\Omega \cdot \text{cm}^2)$	218210	19235	6136
$W_o-T(\Omega^{-1} \cdot \text{cm}^{-2} \cdot \text{s}^{-n})$	953.5	67.53	72.66
W_o-P	0.44117	0.53156	0.54007
Chi-Squared Distribution	3.0383E-3	3.2418E-3	1.0357E-3

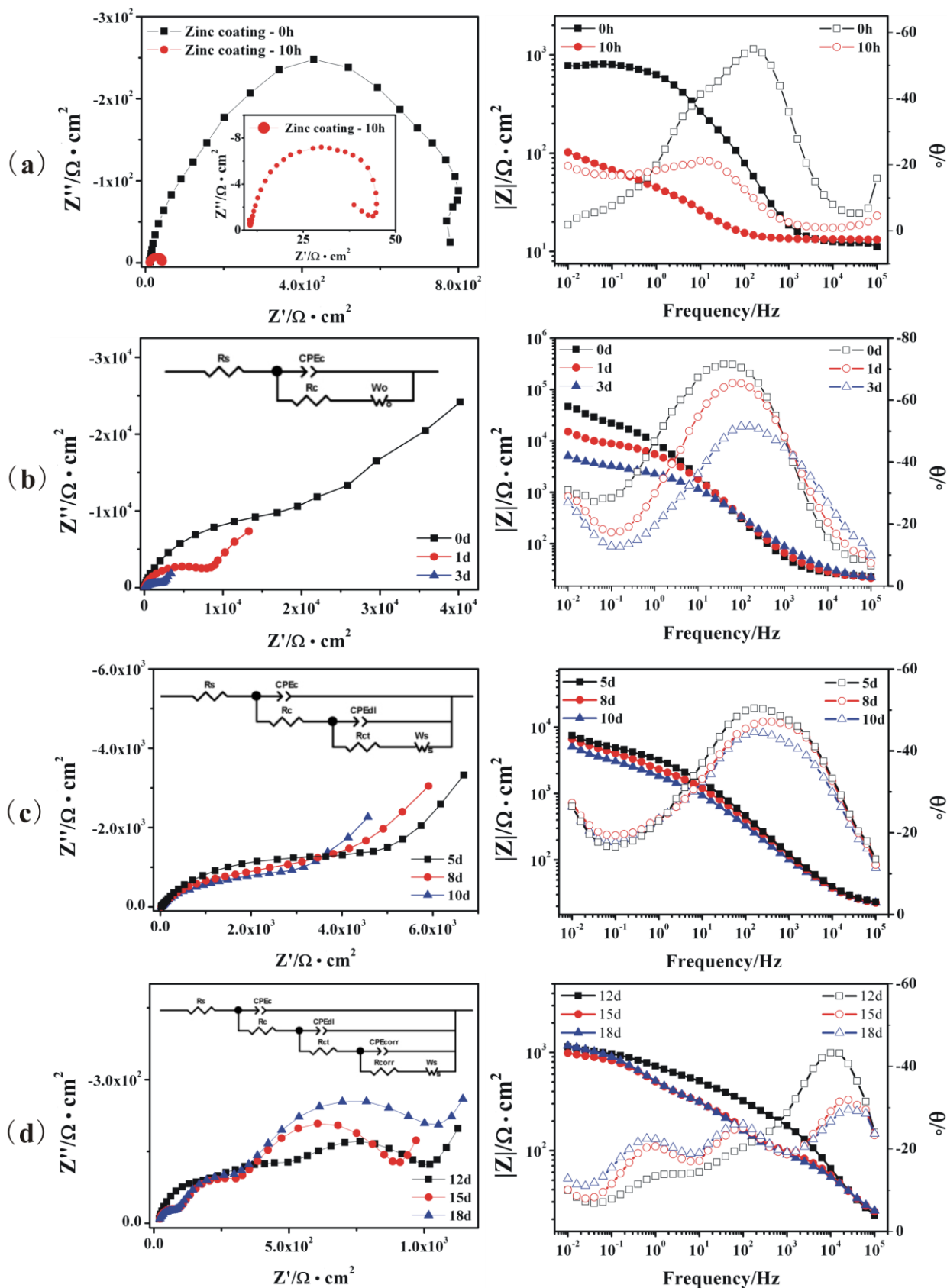


Figure 6. EIS plots of untreated and treated zinc coatings for different immersion time, (a) zinc coating, and (b, c, d) conversion coating.

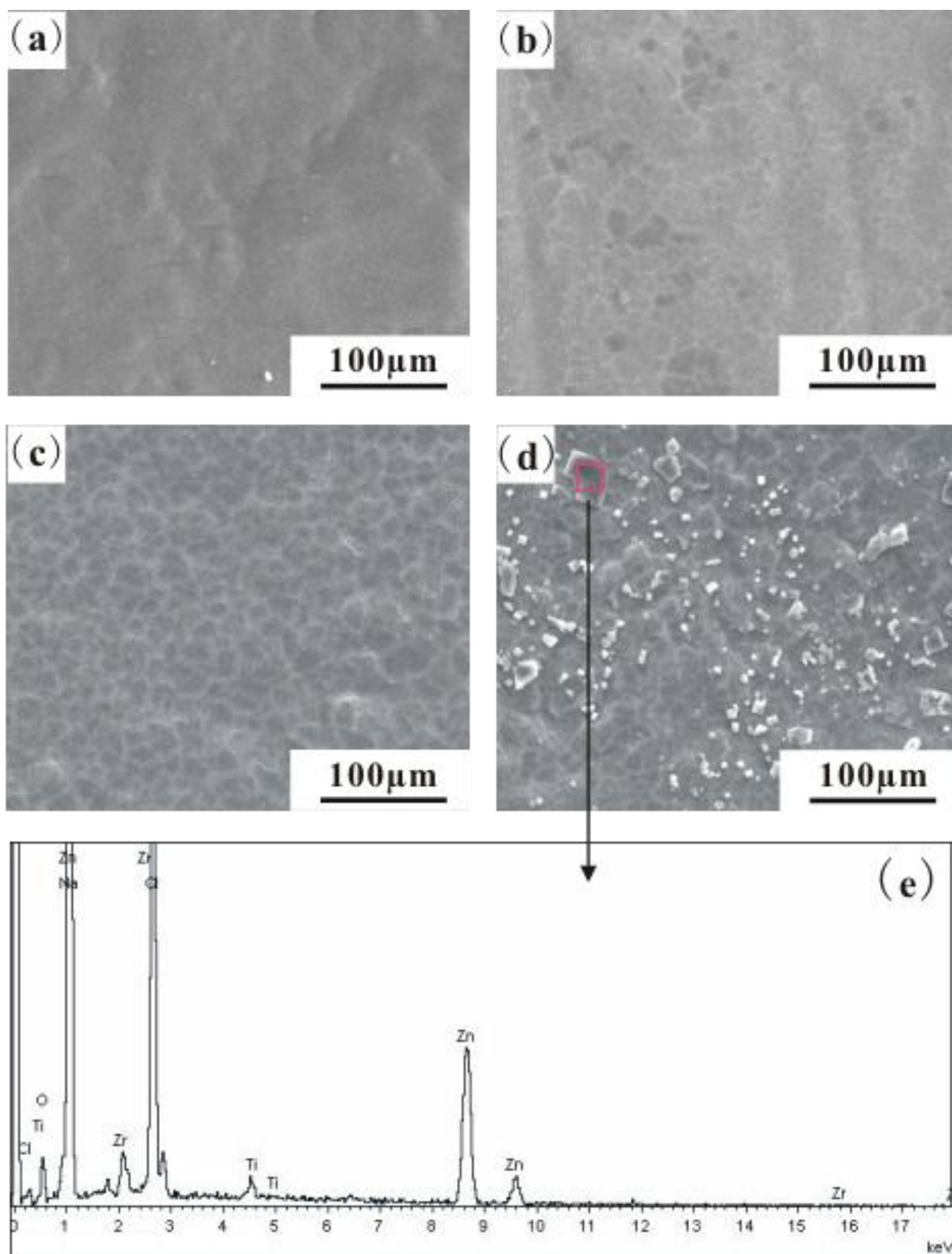


Figure 7. Untreated and treated zinc coatings for different immersion days, (a) before immersion, (b) 3 days, (c) 10 days, (d) 18 days, and (e) EDS analysis after 18 days.

Table 3. EIS fitting results of the conversion coating at the middle immersion stage.

	5d	8d	10d
$R_s(\Omega \cdot \text{cm}^2)$	18.93	18.27	18.23
$\text{CPE}_c\text{-T}(\Omega^{-1} \cdot \text{cm}^{-2} \cdot \text{s}^{-n})$	3.5645E-5	3.9077E-5	3.959E-5
$\text{CPE}_c\text{-P}$	0.63037	0.6259	0.62458
$R_c(\Omega \cdot \text{cm}^2)$	3707	2106	2186
$\text{CPE}_{dl}\text{-T}(\Omega^{-1} \cdot \text{cm}^{-2} \cdot \text{s}^{-n})$	2.3343E-4	2.7775E-4	2.4515E-4
$\text{CPE}_{dl}\text{-P}$	0.75732	0.53137	0.59788
$R_{ct}(\Omega \cdot \text{cm}^2)$	1803	4100	2963
$W_s\text{-R}(\Omega \cdot \text{cm}^2)$	16011	20801	9826
$W_s\text{-T}(\Omega^{-1} \cdot \text{cm}^{-2} \cdot \text{s}^{-n})$	126.9	160.1	78.45
$W_s\text{-P}$	0.64127	0.67723	0.56155
Chi-Squared Distribution	1.8964E-4	2.2767E-4	2.9319E-4

Table 4. EIS fitting results of the conversion coating at the final immersion stage.

	12d	15d	18d
$R_s(\Omega \cdot \text{cm}^2)$	15.73	11.02	7.866
$\text{CPE}_c\text{-T}(\Omega^{-1} \cdot \text{cm}^{-2} \cdot \text{s}^{-n})$	3.2192E-6	1.799E-5	4.893E-5
$\text{CPE}_c\text{-P}$	0.76835	0.60993	0.51877
$R_c(\Omega \cdot \text{cm}^2)$	196.8	110.8	118.9
$\text{CPE}_{dl}\text{-T}(\Omega^{-1} \cdot \text{cm}^{-2} \cdot \text{s}^{-n})$	1.1462E-4	4.7767E-5	4.5409E-5
$\text{CPE}_{dl}\text{-P}$	0.57568	0.80913	0.81605
$R_{ct}(\Omega \cdot \text{cm}^2)$	419.9	227.2	240.9
$\text{CPE}_{corr}\text{-T}(\Omega^{-1} \cdot \text{cm}^{-2} \cdot \text{s}^{-n})$	8.1032E-4	8.79E-4	9.1615E-4
$\text{CPE}_{corr}\text{-P}$	0.69818	0.71775	0.68775
$R_{corr}(\Omega \cdot \text{cm}^2)$	412.9	599.8	774.6
$W_s\text{-R}(\Omega \cdot \text{cm}^2)$	2615	3364	10068
$W_s\text{-T}(\Omega^{-1} \cdot \text{cm}^{-2} \cdot \text{s}^{-n})$	1131	1220	4523
$W_s\text{-P}$	0.60098	0.73669	0.68569
Chi-Squared Distribution	2.2008E-4	9.0451E-4	7.0842E-4

4. CONCLUSIONS

A novel Ti/Zr based non-chromium conversion coating is developed for protecting the electrogalvanized steel. The well-distributed particles on the conversion coating have an average size about 80 nm, and the coating thickness is around 500 nm. The coating comprises five elements, that are, Zn, Ti, Zr, O and F. The coating phases are consisted of complicated oxides or hydroxides of Zn, Ti, Zr elements and zinc fluoride, some of which may be amorphous phases. The mechanism of conversion coating formation is composed of three steps, first zinc coating substrate dissolves, next

conversion coating forms, and then hydrated zinc fluoride generates. Corrosion reaction of the conversion coating is mixed-controlled by charge transition and diffusion through the three immersion stages, and the conversion coating can greatly cut down the corrosion rate of the electrogalvanized steel substrate.

References

1. X.G. Zhang, Corrosion and Electrochemistry of Zinc, China Metallurgical Industry Press, Beijing, 2008.
2. J.W. Bibber, *J. Appl. Surf. Finish.* 2(4)(2007)274.
3. D.L. Correll, *J. Environ. Qual.* 27(1998)263.
4. N.T. Wen, C.S. Lin, C.Y. Bai, M.D. Ger, *Surf. Coat. Technol.* 203(2008)317.
5. G.M. Treacy, G.D. Wilcox, M.O.W. Richardson, *J. Appl. Electrochem.* 29(1999)647.
6. M.F. Montemor, A.M. Simõesa, M.G.S. Ferreira, *Prog. Org. Coat.* 44(2)(2002)111.
7. J. Creus, F. Brezault, C. Rebere, M. Gadouleau, *Surf. Coat. Technol.* 200(14-15)(2006)4636.
8. M.F. Montemora, R. Pinto, M.G. S. Ferreira, *Electrochim. Acta* 54(2009)5179.
9. M. Hara, R. Ichino, M. Okido, N. Wadab, *Surf. Coat. Technol.* 169-170(2003) 679.
10. Y.K. Song, F. Mansfeld, *Corr. Sci.* 48(2006)154.
11. D.Q. Zhu, W.J. van Ooij, *Electrochim. Acta* 49(2004)1113.
12. O. Lunder, C. Simensen, Y. Yu, K. Nisancioglu, *Surf. Coat. Technol.* 184(2-3)(2004)278.
13. A.R. Phani, F.J. Gammel, T. Hack, H. Haefke, *Mater. Corros.* 56(2)(2005)77.
14. OKI. M, *J. Appl. Sci. Environ. Manage.* 11(2)(2007)187.
15. M.F. Montemor, W. Trabelsi, S.V. Lamaka, K.A. Yasakau, M.L. Zheludkevich, *Electrochim. Acta* 53(2008)5913.
16. N. Suzuki, S. Karuppuchamy, S. Ito, *J. Appl. Electrochem.* 39(2009)141.
17. S.H. Wang, C.S. Liu, F.J. Shan, *Acta. Metall. Sin.(Engl. Lett.)* 22(3)(2009)161.
18. A.S. Hamdy, M. Farahat, *Surf. Coat. Technol.* 204(2010)2834.
19. L.Y. Wu, J.B. Lian, G.X. Sun, X.R. Kong, W.J. Zheng, *Eur. J. Inorg. Chem.* 20(2009)2897.
20. H.Y. Xu, Y.C. Liu, J.G. Ma, Y.M. Luo, Y.M. Lu, D.Z. Shen, J.Y. Zhang, X.W. Fan, R. Mu, *J. Phys.: Condens. Matter* 16(28)(2004)5143.
21. A. Pilbáth, I. Bertóti, I. Sajó, L. Nyikos, E. Kálmán, *Appl. Surf. Sci.* 255(2008)1841.
22. U. Vohrer, H.-D. Wiemhöfer, W. Göpel, B.A. van Hassel, A.J. Burggraaf, *Solid State Ionics* 59(1993)141.
23. C. Malitesta, I. Losito, F. Scordari, E. Schingaro, *Eur. J. Mineral.* 7(1995)847.
24. J. Lin, H. Y. Chen, L. Chen, K.L. Tan, H.C. Zeng, *Appl. Surf. Sci.* 103(1996)307.
25. W. Wang, H.T. Guo, J.P. Gao, X.H. Dong, Q.X. Qin, *J. Mater. Sci.* 35(2000)1495.
26. R.A. Espinoza-González, D.E. Diaz-Droguett, J.I. Avila, C.A. Gonzalez-Fuentes, V.M. Fuenzalida, *Materials Letters* 65(2011) 2122.
27. J.C. Dupin, D. Gonbeau, P. Vinatier, A. Lévassieur, *Phys. Chem. Chem. Phys.* 2(2000)1319.
28. H.K. Kim, T.Y. Seong, K.K. Kim, S.J. Park, Y.S. Yoon, I. Adesida, *Jpn. J. Appl. Phys.* 43(2004)976.
29. U. Müller, R. Hauert, *Thin Solid Films*, 290-291(1996)323.
30. J. Zhang, G.H. Li, *Solid State Phenomena*, 121-123(2007)1273.
31. Y. Kuroda, T. Morimoto, *Langmuir*, 4(2)(1988)430.
32. K. Nakamoto, *Infrared and Raman Spectra of Inorganic and Coordination Compounds*, John Wiley & Sons, 1978.
33. G. Liu, C.H. Sun, L.N. Cheng, *J. Phys. Chem., C*, 113(2009)12317.

34. J.G. Wu. *Technology and Application of Modern FTIR Spectroscopy* (Vol. 1), Science and Technology Literature Press, Beijing, 1994.
35. C.C. Hu, *Fundamentals and Methods of Electrochemistry*, Wunan Book Co., Ltd, Taipei, 2002.
36. C.N. Cao, J.Q. Zhang, *An Introduction to Electrochemical Impedance Spectroscopy*, Science Press, Beijing, 2002.
37. U. Rammelt, G. Reinhard, *Corr. Sci.* 27(1987)373.
38. A.Conde, J. de. Damborenea, *Electrochim. Acta* 43(1998)849.